# Convergent Hydrodynamics of Inertial Confinement Fusion Implosions

*C. W. Barnes, J. A. Oertel, and R. G. Watt (P-24);*
*R. E. Chrien (P-22);*
*J. B. Beck, N. D. Delamater, and D. L. Tubbs (X-TA);*
*N. M. Hoffman (X-CI);*
*H. Bush, R. D. Day, S. Dropinski, J. Duke, P. Gobby, V. Gomez, D. Hatch, R. Manzanares, J. Moore, and G. Rivera, (MST-6 and MST-7);*
*M. J. Edwards, W. W. Hsing, J. D. Colvin, O. L. Landen, and B. A. Hammel (Lawrence Livermore National Laboratory);*
*C. J. Keane (DOE);*
*D. Galmiche and A. Richard (DRIF/CEA, France);*
*M. Dunne, P. Graham, S. Rothman, and B. Thomas (AWE, United Kingdom);*
*T. R. Boehly, D. K. Bradley, P. Jaanimagi, and J. P. Knauer (Laboratory for Laser Energetics, University of Rochester);*
*D. Haynes and C. Hooper (University of Florida);*
*S. A. Voss (University of New Mexico); and*
*N. A. Shambo (North Carolina State University)*

## Introduction

The National Ignition Facility[1] (NIF), a large laser presently under construction at the Lawrence Livermore National Laboratory, is designed to produce 1.8 MJ of 0.35-μm light in a 500-TW pulse for defense applications and inertial fusion ignition. Although fundamental questions about the feasibility of achieving high gain in inertial fusion capsule implosions were settled a decade ago in a series of underground experiments at the Nevada Test Site, it remains a major scientific and technical challenge to obtain capsule ignition and gain in the laboratory with the laser energy and power available at the NIF.

Inertial fusion ignition and gain requires that a fuel region with enough size and density be heated to a high temperature such that fusion burn can be transiently sustained by energy deposited by the charged fusion reaction products. Ignition is easiest to obtain using a deuterium-tritium fuel mixture, and for this fuel the requirements are a temperature of about 20 keV and a density-radius product of a few $g/cm^2$. Rather than producing these conditions in a uniform volume (which would require a laser energy on the order of 100 MJ), the mainline capsule design for the NIF employs a concept known as "hot-spot" ignition. In this concept, a small fraction of the fuel mass is ignited in a central hot spot, and then a thermonuclear burn wave propagates outward into the surrounding compressed fuel to produce a significant fusion yield.[1]

Hydrodynamic perturbation growth during the capsule implosion plays a major role in determining whether the hot spot in the fuel can ignite. Hydrodynamic instabilities pose a threat to ignition by creating spikes of cold fuel that penetrate into the hot spot and increase thermal losses from this region. The energy required to ignite a capsule increases as shell thickness increases, and the minimum acceptable shell thickness depends on the magnitude of the perturbation growth that would disrupt the shell. Hydrodynamic instabilities can also reduce the efficiency with which the kinetic energy of the imploding shell (or "pusher") is converted to temperature of the hot spot and reduce the overall compression of the fuel. Another mechanism that could affect ignition is the introduction of contaminants from the shell into the fuel (a process known as "mix") and subsequent radiative energy loss.

Perturbations occur because of nonuniformities in the radiation drive on the shell or fuel surface. During the ablative acceleration phase, perturbations at the ablation front grow via the Rayleigh-Taylor instability, whereby the lower-density ablated material accelerates the higher-density unablated shell. These perturbations are transferred or "fed through" to the inner surface of the shell, where they can further grow during the convergence and deceleration phases (see Fig. 1). These inner surface perturbations cause mix of the cold ablator with the hot fuel, either preventing ignition or, conversely, increasing the size of the driver required to achieve a fixed gain.

Because the Rayleigh-Taylor instability at the ablation front is expected to be the dominant effect for inertial confinement fusion (ICF) implosions, there has been much effort devoted to theoretical development and measurement of the instability under ICF-relevant

conditions. However, few experiments have explored the effects of ablatively driven Rayleigh-Taylor growth in convergent geometries. Calculations of the hydrodynamic performance of ignition capsules[2] for the NIF need to be validated by present-day experiments. To address this issue, the Laboratory's ICF Program has launched two campaigns to explore the growth of hydrodynamic instabilities in cylindrical and spherical geometries. This research highlight describes each of these research efforts with an overview of the results.

## Cylindrical Implosion Research on the Ablative Rayleigh-Taylor Instability

Cylindrical implosions can provide physical insight into convergent hydrodynamics issues because cylindrical geometry allows for excellent diagnostic access along a line of sight and provides a good match to present two-dimensional (2-D) simulation codes. By contrast, in a spherical implosion along any diagnostic line of sight, material is moving towards, away from, and across the diagnostic. Unfolding the radial dependence of the implosion from such line-integrated observations is difficult. Thus, spherical implosion experiments usually rely on "integrated" measurements of the performance of the implosion. In a cylindrical implosion, the diagnostic view along the cylindrical axis only has material moving at right angles to the field of view and the radial unfolding of the information is straightforward. With proper design of the axial implosion, the experiment can be kept relatively 2-D and thus tractable for detailed comparison to present-generation simulation codes. Convergent effects are not as strong in a cylindrical implosion (only increasing as $1/R$ and not $1/R^2$ as in a spherical implosion), but those effects can still be effectively studied.

Our early research focussed on cylindrical implosions using indirect-drive at Livermore's Nova laser.[2,3] Experiments were conducted using a cylinder that extended transversely across the entire diameter of a Nova hohlraum, which was driven using eight Nova beams with a total energy of 22–25 kJ (Fig. 2). The eight beams were arranged symmetrically around the cylinder in the hohlraum to provide the best possible drive symmetry although there still was an initial m = 4 azimuthal variation of illumination. The implosions were radiographed axially using a gated x-ray pinhole imaging system and a silver or titanium backlighter foil on the far side.
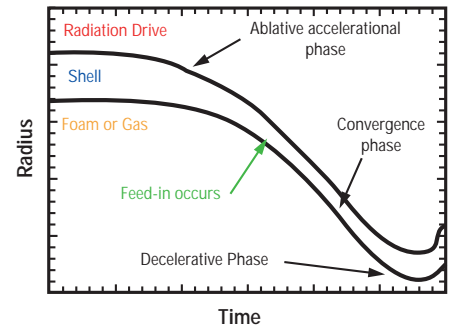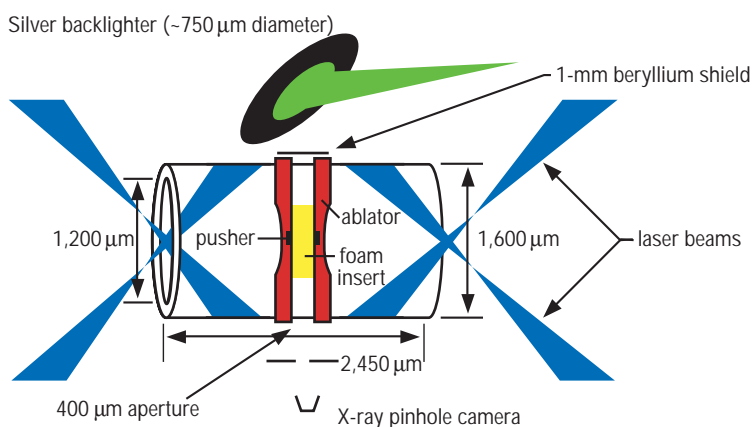


*Fig. 1  Phases of hydrodynamic instability during an implosion. Perturbations on the outside of the shell are fed through to the inner surface, where they grow as the implosion progresses.*



*Fig. 2  Experimental design for an indirect-drive experiment on Nova. The cylinder is mounted transversely across the diameter of the hohlraum. Eight laser beams are arranged symmetrically around the cylinder and drive its implosion with an energy of 22–25 kJ. The x-ray pinhole imaging system (which includes the backlighter, beryllium shield, aperture, and pinhole camera) provides axial radiographs of the imploding cylinder.*
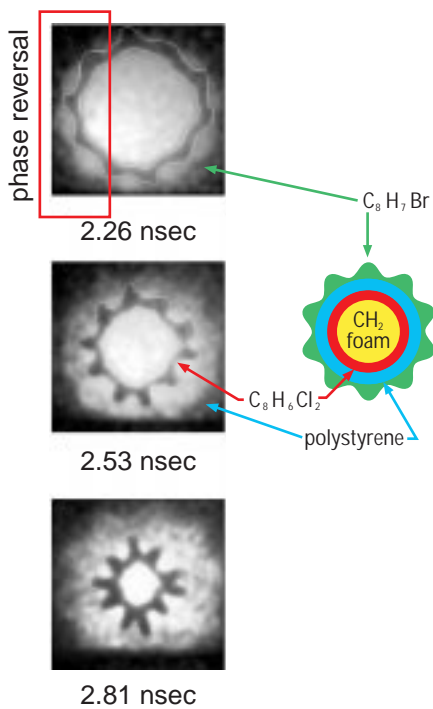
Fig. 3  *Sequence of gated x-ray framing camera images from an indirectly-driven cylindrical implosion at Nova. The dark, convoluted region comes from feed-in of perturbations growing at the ablation surface to a marker region of chlorinated plastic. The dark region at the outside is ablated brominated plastic. The lighter area between these layers is the polystyrene ablator. (Diagram of layers is not to scale.)*

The cylinder design primarily used in these experiments had a 472-μm outer diameter, and it comprised a brominated polystyrene ablator over a plain polystyrene pusher with a 60-mg/cc, 430-μm-inner-diameter, polystyrene foam insert. The cylinder was shielded by gold coating at its ends and was tapered along its length so that only an approximate 300-μm waist region imploded. The axial length was further defined by a thin, 160-μm-long chlorinated polystyrene marker layer between the pusher and the foam; however, further tests have confirmed that most of the radiographic contrast comes from radial densification of the implosion and not from the opacity of the chlorinated marker. Perturbations were machined azimuthally on the outside of the ablator.[4]

A sequence of over 20 targets was shot at Nova with nearly identical conditions. Only the azimuthal mode number (either m = 10 or m = 14) or amplitude (unperturbed, 0.25, 0.5, 1.0, 1.5, 3.0, and 5.0 μm) of the machined perturbation varied. (The mode number is the number of perturbation wavelengths around the circumference of the cylinder.) An example of the sequence of data provided from a single shot is shown in Fig. 3. These experiments provided valuable data for all three phases of instability growth during cylindrical implosions. There is a clear indication of phase reversal at the ablation surface (the outer dark region).

The first phase of the implosion consists of initial ablative Rayleigh-Taylor instability growth at the ablation front, in which the perturbations feed into the marker region (which has a higher compressed density at the plastic-foam interface). The ratio of the final measured perturbation amplitude and initial machined perturbation amplitude is the measured growth factor. In these initial indirect-drive experiments, the acceleration tended to occur only while the convergence ratio was less than about 1.5. The measurements of instability growth occur at or after the time this convergence is reached. Hence the ablative Rayleigh-Taylor instability growth sets the initial amplitude observed in the experiment. Our experiments confirm the expectation that the mode m = 14 grows faster and to higher amplitude than the m = 10. Perturbations with initial amplitude 1.5 μm or less remained linear during the ablative Rayleigh-Taylor phase, and the growth factors for the same mode number were the same during the entire implosion. Detailed time-dependent measurements of mode amplitudes can then be compared to hydrodynamic simulations. A post-processing code is used to simulate the x-ray radiographs from calculations with LASNEX, a 2-D radiation hydrodynamics code, using the same filtering and analysis as done in the experimental data reduction (see Fig. 4).

In the second phase, convergence, the perturbations continue to grow even in the absence of acceleration. This "crenulation" effect, first identified by Bell[5] and Plesset[6], is a feature of all convergent implosions that act incompressibly. For a ring or shell of material to maintain its volume as it converges, it must thicken and its wrinkles must grow. In our experiments, all of the perturbations appeared to grow at the same rate regardless of size, even when the perturbations exceeded usual "nonlinearity conditions" (*e.g.*, even when the amplitude was a

significant fraction of the wavelength or radius). The largest initial amplitude perturbations did show signs of saturation in their growth, but not until they reached amplitudes divided by wavelength of nearly unity! Examples of the different nonlinear shapes that result from starting with increasing initial amplitude are shown in Fig. 5. These nonlinear effects were studied in detail using a target with the largest initial amplitude yet tried, an m = 10, 5-μm perturbation. This amplitude was chosen to go nonlinear during the ablative Rayleigh-Taylor phase. Several features are seen in these images. First, the rod-like spikes grew steeper and, for the first time in these experiments, developed observable harmonics of the fundamental. The image also shows that, late in time, the spikes "crush in" from the compressibility effects of Bell-Plesset growth.

During these first two phases of the implosion, there is second-order, weakly nonlinear mode coupling between the machined perturbations and the m = 4 illumination asymmetry caused by the eight laser beams in the hohlraum. This leads to m = 10 + 4 = 14 and m = 10 - 4 = 6 modes with phases and amplitudes that appear consistent (within factors of two) with theory[7] when derived for convergent geometry. This mode coupling creates the "lumpy" look of the data, which is not noise, but actually an important feature of the physics.

In the third phase, deceleration, there is expected to be Rayleigh-Taylor growth at the unstable pusher-foam interface. However, three-dimensional (3-D) end effects in the target design made the interface inside the marker layer diffuse and such effects were not seen. At the outside of the marker layer, compressibility effects[3] reduced the size of the perturbations.

To improve upon the Nova experiments, we collaborated with scientists from the University of Rochester on a series of experiments to study convergent hydrodynamics using direct-drive illumination at the Laboratory of Laser Energetics Omega facility.[8] The use of direct-drive illumination couples more energy into an implosion (perhaps 10 kJ out of 18 kJ of ultraviolet laser light instead of 3 kJ from the



(a)

(b)
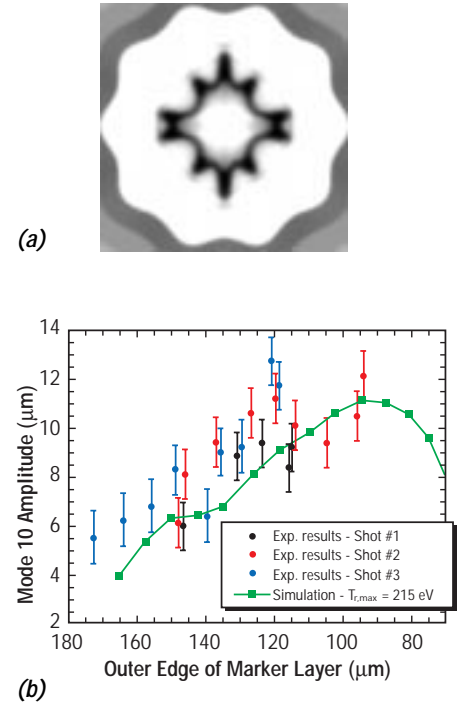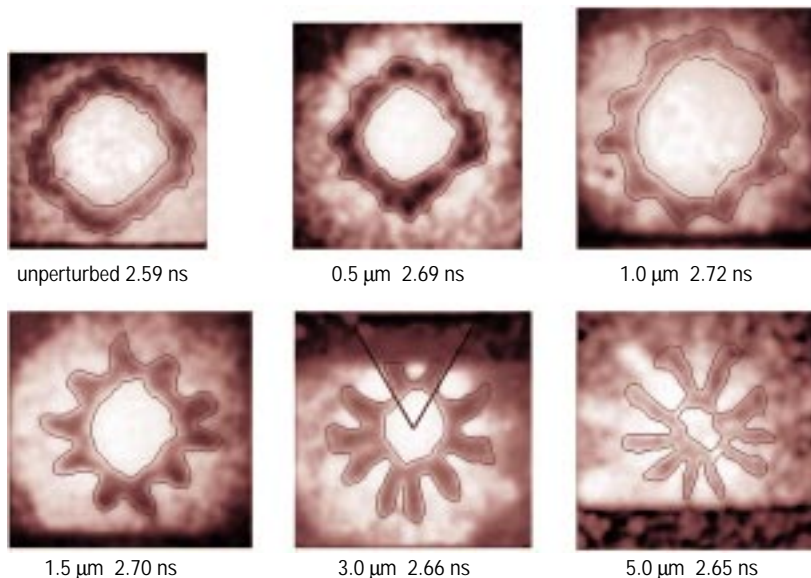
Fig. 4 Post-processed simulation of an axial x-ray radiograph generated from a hydrodynamic simulation of an indirect-drive cylindrical implosion on Nova (the image includes m = 4 illumination asymmetry). (b) Comparison of simulated amplitude and experimental measurements from m=10, 1-μm initial amplitude perturbations. The simulations fit well with the experimental results.



unperturbed 2.59 ns          0.5 μm 2.69 ns          1.0 μm 2.72 ns

1.5 μm 2.70 ns          3.0 μm 2.66 ns          5.0 μm 2.65 ns

Fig. 5 Images at similar times (and hence radii) of cylindrical implosions, starting from different initial perturbation amplitudes. Varying the starting amplitude produces widely different nonlinear shapes.

*Fig. 6   Photograph of the cylinder used in direct-drive experiments on Omega. The cylinder is aligned along the diagnostic axis and includes components of the imaging system (axial backlighter, leaded acrylic aperture, and various alignment fibers).*
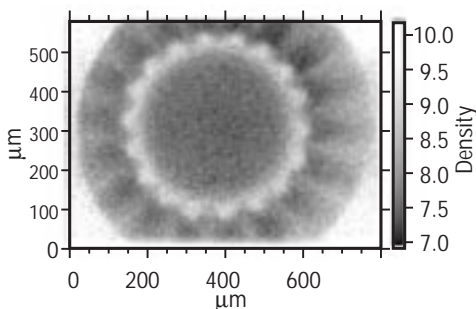


*Fig. 7   X-ray radiograph from a "feed-out" test using direct-drive cylindrical implosion on Omega. The experiment used a cylinder with m = 18, 1.5-µm amplitude perturbations on the interior surface of the ablator. These perturbations "fed-out" to the ablation front and grew as the implosion progressed.*

indirect-drive x-ray radiation for a similar amount of ultraviolet laser energy). Thus, we were able to implode cylinders that were twice as large as the ones used in the Nova experiments with corresponding increases in convergence ratio at maximum acceleration (2.5 instead of 1.5), growth factors (30 instead of 15), and resolution (nearly twice the pixel resolution elements at the same convergence). Using direct drive advances in smooth beam illumination (distributed phase plates and smoothing by spectral dispersion) we achieved generally more symmetric implosions with less mode coupling as well.[9]

The cylinders used in the Omega experiments (see Fig. 6) were unique because of their thin-wall construction. With an inside diameter of 860 µm and a wall of 20 µm, these polystyrene cylinders were particularly fragile. To ensure their survival, the polystyrene-coated mandrels were annealed three times prior to final mandrel removal. The outer surface of the cylinders was machined with azimuthal modes varying with m = 14, 28, 38, or 58, with amplitudes from 0.5 to 1 µm. The 2.25-mm-long plastic cylinders were coated with 500 Å of aluminum that served as a shine shield to provide uniform plasma breakdown. They were filled with 60 mg/cc polystyrene foam; some targets had the foam doped with deuterium or chlorine to enhance neutron or spectroscopic diagnostic measurements. Extensive metrology of the completed targets (measuring angles to within 0.1° and position to within a few µm) ensured that the Omega beams provided the illumination required and that all of the beams hit the target.

During the Omega experiments, 50 laser beams were focussed around a central band of the cylindrical target. Very symmetric implosions were achieved with convergence ratios of seven for the shell and 10 for the hot spot or axial emission spike. Twenty-two shots were obtained in this first scoping campaign, including 17 implosions, 15 of which had both excellent energy and power balance. Thirty-four shots were obtained in the second campaign including 28 implosions scoping out a variety of experimental and theoretical issues. On each shot, five to eight of the remaining laser beams were focussed on titanium backlighters. X-ray radiography was performed both axially and transverse to the cylinder axis to produce excellent sets of gated framing camera images of the hydrodynamics of the cylinder imploding.[10] Results from one experiment are shown in Fig. 7. In addition, framing and streaked images and time-resolved x-ray spectroscopy were used to explore the behavior of these targets.

During this campaign, we modified two of the target cylinders to allow for study of perturbations on the interior surface. The image in Fig. 7 shows an x-ray radiograph from this experiment. Perturbations with m = 18 and 1.5 µm amplitude were put on the inside surface of the ablator at the foam interface. The results from these interior perturbation experiments can be used to study the "feed-out" problem associated with the Rayleigh-Taylor instability.[11] In this process, the initial shock driven through the ablator reflects off the rippled surface at the inside and bounces back to the ablation front where it seeds instability growth there.

Detailed analysis of these experiments and design for future campaigns continues, now in additional collaboration with researchers from the Atomic Weapons Research Establishment in the United Kingdom and from the University of Florida. These results are providing high quality data useful for validation of complex hydrodynamic calculations such as those used to predict ignition at the NIF.[12] Figure 8 shows comparisons of measured mode amplitude with LASNEX simulations, showing disagreement late in the acceleration history with the predicted mode growth. Current work concentrates on understanding and ameliorating the effects of short-wavelength laser nonuniformities on the perturbation growth; measuring the "thermodynamics" of the cylindrical implosions by spectroscopic or neutronic methods for comparison to the observed hydrodynamics; and observing mix and defect evolution at the inside interface of the ablator.

## Spherical Capsule Implosions using a Deuterated Layer

While experiments such as those described above provide useful information about perturbation growth, ignition capsules designed for the NIF are, in general, much more unstable than cylindrical (and most spherical) implosions studied in Nova and Omega experiments. In the absence of nonlinear effects that reduce the perturbation growth rate, the spikes of cold pusher material penetrating into the hot-spot region of these NIF capsules are predicted to be ~400-times larger than the initial perturbations on the capsule surfaces (this is known as the linear growth factor). Fortunately, nonlinear processes reduce the perturbation growth and thus the size of the spikes. In order to test the ability of our computer simulations to predict the *actual* levels of perturbation growth in NIF capsules, a series of spherical capsule implosions on Nova was designed to maximize the perturbation growth and produce linear growth factors at levels as close as possible to those expected in ignition capsules on NIF.

These high-growth Nova implosions, designed by Keane[13] and performed by Hammel and Landen[14], enhanced the perturbation growth by using a germanium dopant in the pusher, producing linear growth factors of ~100. The main diagnostic of capsule performance was the neutron yield from deuterium gas filling the capsule (Fig. 9a). In these Nova implosions, the three deleterious effects of perturbation growth (enhanced thermal losses, mix, and reduced compressional heating) all act to cool the deuterium fuel so that their relative



*(a)*



*(b)*
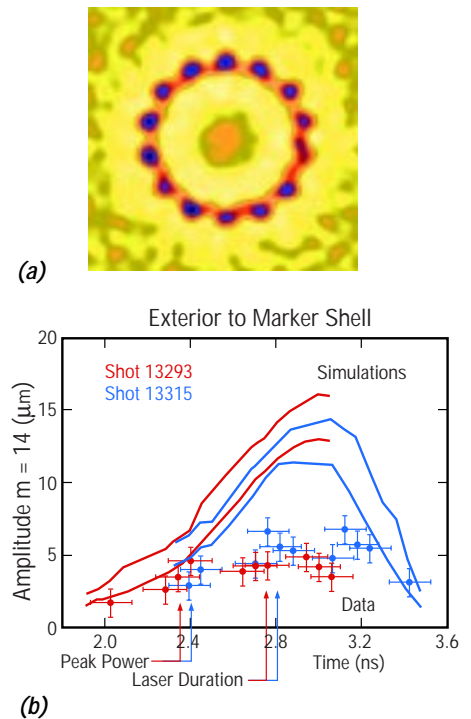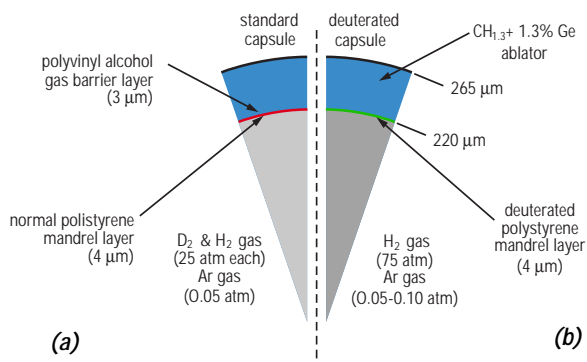
*Fig. 8  (a) Post-processed simulation of an x-ray radiograph generated from a hydrodynamic calculation, including the effects of finite photon statistics. (b) Comparison of simulated and experimental measurements of mode and amplitude for an m = 14, 0.5-μm initial amplitude perturbation. The amplitude is measured at the interface exterior in radius to the chlorinated marker shell. There is disagreement in the predicted and actual mode growth late in the acceleration history.*



*(a)*                    *(b)*

*Fig. 9  Pie diagram of the standard deuterium-filled capsule (a) and the hydrogen-filled deuterated-shell capsule (b). In (a) the neutron yield is produced in the compressed deuterium gas region, while in (b) it is produced in the deuterated inner layer of the pusher heated by thermal conduction from the nonreacting gas. Higher linear growth factors are produced in capsule (b), approaching the values calculated for NIF capsules.*

importance cannot be separated through a neutron yield measurement. However, we realized that in capsules made with a deuterated inner layer and filled with nonreacting hydrogen gas (Fig. 9b), increased heat loss and atomic mix would both *increase* the temperature of the deuterated layer. These deuterated shell capsule implosions would be sensitive to the interface between the pusher and the gas, but relatively insensitive to the compressed gas region. As a result, deuterated shell implosions would provide an additional and qualitatively different constraint on simulations that would be complementary to the deuterium-filled, high-growth capsule implosions and would help to determine the relative importance of the effects of perturbation growth. A series of implosions using deuterated shell capsules was performed. As described below, these implosions reached linear growth factors of ~325, approaching those predicted for NIF capsules.

The capsules were imploded by indirect x-ray drive on the Nova[15] laser using a shaped, 2.2-ns-long laser pulse with 31 kJ of energy. The capsules were mounted in 2.40-mm-long, 1.65-mm-diameter pentagonal hohlraums. The laser pulse produced a peak radiation temperature of 232 eV in the hohlraum. As shown in Fig. 9b, the capsule shells included a germanium dopant to reduce preheat of the pusher and the gas by gold *M*-band x-rays from laser-plasma interactions at the hohlraum wall, steepen the density gradient at the ablation front, and reduce the ablation rate.[16] These effects increased the perturbation growth from hydrodynamic instabilities to values approaching those calculated for NIF capsules.

To study the effect of perturbation growth on capsule performance, we varied the surface roughness of the shells by laser ablation pitting.[17] The roughness was varied by adjusting the laser energy to control the depth of the pits, and the surface perturbations were measured by atomic force microscopy.[17] The power spectrum of the surface perturbations (Fig. 10) can be used as a starting point for hydrodynamic stability calculations. The most dangerous modes are

*Fig. 10    One-dimensional power spectra for smooth and laser-roughened capsules, which can be used as a starting point for hydrodynamic stability calculations. Mode numbers below 10 have much slower predicted growth rates and are excluded from calculations by substituting the power in mode 10, as indicated by the dashed lines.*
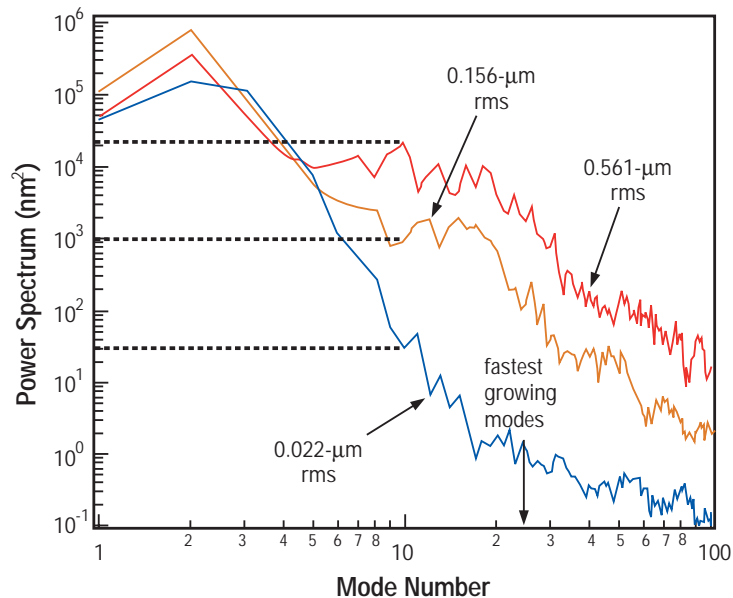
expected to be those with wavelengths similar to the capsule thickness. As a simple measure of the surface roughness, the power spectrum is also summed to obtain the surface variance and, from the square root of the variance, the root-mean-square (rms) surface roughness. Low mode numbers (below 10) have much slower calculated growth rates than modes in the range 10–30 and are excluded from the surface variance summation by substituting the power in mode 10 for the power in modes 1–9.

The observed dependence of yield on surface roughness is shown in Fig. 11. The neutron yields are obtained from Nova's Tion[18] and LaNSA[19] single-interaction neutron detector arrays located at 27 m and 20 m, respectively, from the target. The neutron yields are

Legend:
- Experiment
- LMS ($\alpha=0$)
- LMS ($\alpha=1$)
- LMS ($\alpha=1$, 231 eV)
- LMS (1=2,4,...,48)
- LMS (1=24)

Haan "mix" model (fast calculations)

direct numerical simulation (slow calculations)

Neutron Yield vs rms Surface Roughness (μm)
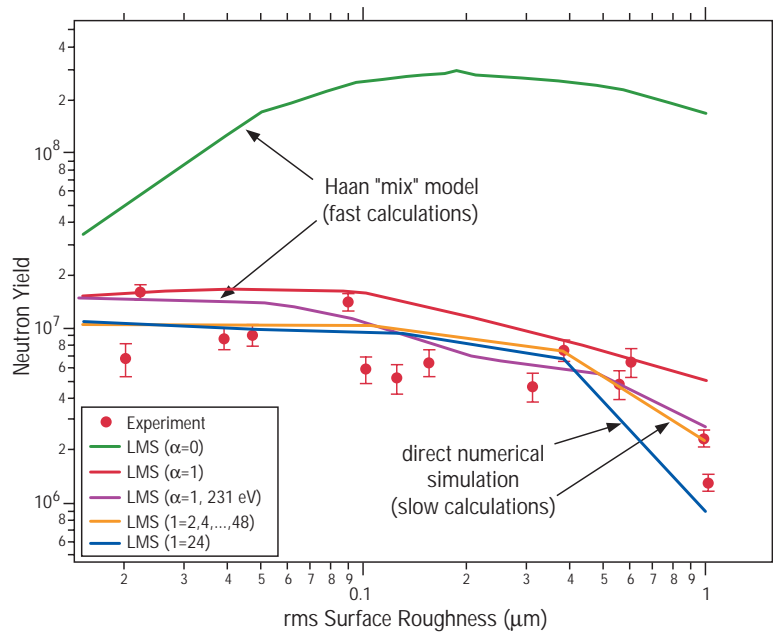
*Fig. 11 Variation of measured and simulated (LMS and DNS) neutron yield with surface roughness. All experimental data points are from the Tion array except two points at 1-μm rms roughness from the LaNSA array. This table illustrates that the simulations fit well with the results except in the case of the LMS $\alpha = 0$ simulation.*

approximately constant for surface roughness up to 0.2 μm and decrease for rougher surfaces. X-ray images (in the 3–4 keV photon energy range) of 1-μm-roughness capsules at peak compression are distinctly larger and weaker than the images at other surface roughnesses (Fig. 12), suggesting that these shells have broken up

**Smooth Capsule** (0.022-μm rms roughness)

(a)

**Rough Capsule** (1.156-μm rms roughness)

(b)
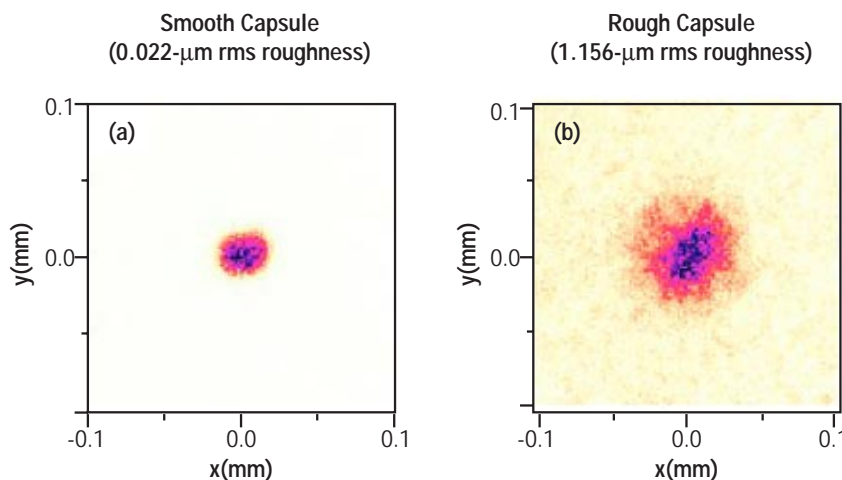
*Fig. 12  Gated x-ray images of smooth and rough capsules at peak compression times. In general, capsules with roughnesses $\geq 1$ μm produced larger, weaker images, suggesting that the capsules broke up during the implosion.*

during the implosion. The image diameters at the 50% intensity contour for the smooth and 1-µm-roughness capsules are $25 \pm 5$ µm and $50 \pm 10$ µm, respectively. The neutron energy spectrum, summed over all the shots, had a full-width-at-half-maximum (FWHM) energy spread of $99 \pm 6$ keV. This energy spread, if caused solely by thermal motion of the deuterons[20], would correspond to an ion temperature $T_i = 1.43 \pm 0.17$ keV. However, the neutrons could also be subject to Doppler broadening from bulk fluid motion[21] during the time of neutron production as a result of the motion of the deuterated layer.

We performed two types of simulations of these implosions. The first type is known as direct numerical simulation (DNS).[22,23] It involves direct calculation of perturbation growth using the LASNEX[24] 2-D radiation hydrodynamics code, starting with a realistic mode spectrum and following the perturbations into the nonlinear regime. Neutron yield and other observables are calculated at the same time as the perturbation growth. The simulation involves no adjustable parameters associated with hydrodynamic instabilities, heat conductivity, or mode saturation. The simulations directly predict the nonlinear "bubble and spike" structures on the inner surface of the capsule which increase the inner surface area and thus heat loss from the gas. Furthermore, DNS explicitly predicts the reduction in compressional heating of the gas as a result of perturbation growth. For small rms roughness, the yield predictions of DNS are nearly independent of roughness and are the same whether they are started with a spectrum of 24 modes ($\ell = 2, 4, \ldots, 48$) or with the same roughness in the dominant mode ($\ell = 24$). However, for large rms roughness (>0.4 µm), when the shell is beginning to break up, the single-mode $\ell = 24$ calculations predict a more rapid decrease in yield than the multimode calculations, as expected for the dominant mode.

*Fig. 13  Variation of DNS calculations of peak compressional heating power (circles) and peak fusion-weighted ion temperature (squares) with capsule surface roughness.*
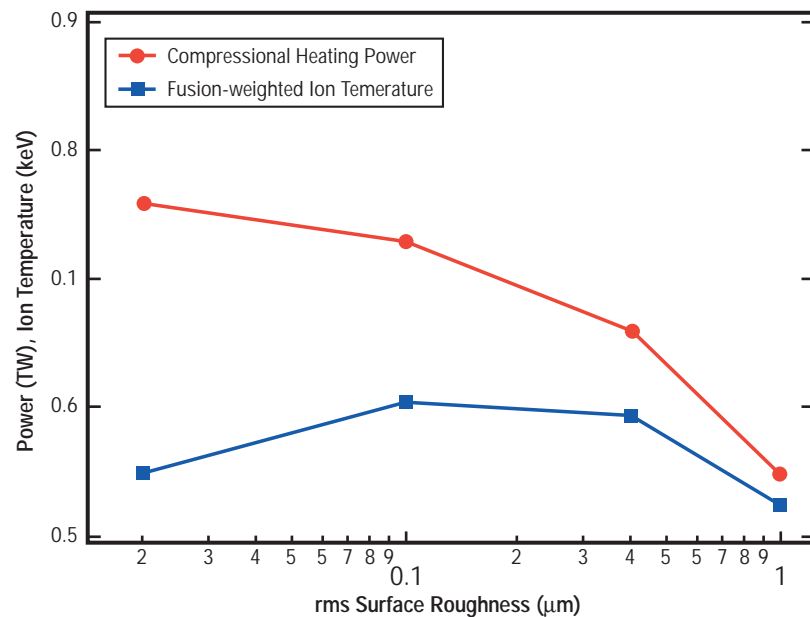
DNS predictions are in quantitative agreement with the measured yields (Fig. 11), and thus provide a confirmation of the method. Both single- and multi-mode DNS yields decrease slowly with surface roughness up to 0.4-μm and then begin to fall more rapidly. The most obvious effect of perturbation growth in DNS is a reduction in the peak compressional heating power. The decrease in compressional heating is partially compensated for by an increase in the temperature of the deuterium. This effect is manifested in DNS as an increase in the fusion-reaction-weighted ion temperature (Fig. 13). The increase in temperature from a smooth implosion to 0.1-μm roughness corresponds to a nearly two-fold increase in fusion reactivity, and is roughly balanced by a similar decrease in the average density of the deuterated layer. These simulations indicate fully developed turbulence and shell breakup for implosions with roughness greater than 0.4 μm, in agreement with the experiments.

DNS predictions for the x-ray image sizes are similar to the experimental observations. The diameter of the x-ray images in the 3–4 keV range at the time of peak emission is predicted to be 29 μm for smooth capsules, increasing to 33 μm for 0.4-μm-roughness and 43 μm for 1-μm-roughness capsules. The maximum intensity of the images is also predicted to decrease by a factor of two from the smooth to the roughest capsules, similar to the trend toward weaker images in the experiments.

The ion temperature inferred from the neutron spectra (1.4 keV) is higher than the DNS predictions and corresponds to a 200-times larger fusion reactivity. To reconcile the measured yields with this temperature, one would have to postulate a 200-fold reduction in the product of deuterium density, inventory, and burn duration. Any such explanation would be difficult to reconcile with simulations of other ICF implosions, which typically match the average measured yield within 30%. On the other hand, mass flows can increase the neutron energy spread without increasing the fusion reactivity. Neutron spectra calculated by post-processing the output of DNS calculations show the qualitative effect of broadening by mass flow, especially in the early part of the burn when spike speeds are largest. Quantitatively, however, the calculated mass-flow broadening integrated over the entire burn duration is insufficient to explain the observed spectral width. This discrepancy may indicate that significant mass-flow broadening occurs at scales too small to be resolved in the calculations, that the symmetry enforced in 2-D single-hemisphere calculations causes unrealistic stagnation of the flow, or that 3-D spikes in the experiment travel faster than 2-D spikes in the calculations. Neutron energy broadening from mass flow may also be important in other ICF experiments whenever deviations from spherical symmetry produce flows in the gas region with speeds approaching $1 \times 10^7$ cm/s during the fusion burn.

The second type of simulation, known as linear mode superposition and saturation (LMS), has been extensively applied to NIF capsule design.[25] It begins with a calculation using LASNEX of the linear growth rates of individual spherical harmonic modes (with infinitesimal amplitudes) seeded at the outer surface. The calculated

linear growth factors (ratios of final and initial mode amplitudes without any mode saturation) are largest for modes between 20 and 24, and reach ~325 at the time of peak neutron emission. The individual modes are superimposed, using the measured initial surface perturbations on the capsule and including a saturation criterion for the growth rate of each mode.[26] The procedure is used to predict the rms amplitude $L$ of the perturbations at the gas-pusher interface throughout the implosion. An annulus of width $L$ is assumed to be mixed on an atomic scale. Once the extent of the mixed region is known, the neutron yield is predicted in a separate one-dimensional (1-D) calculation. Since LMS simulations do not account for increased surface area in the mixed region, an enhancement to the usual electron thermal conductivity is applied in that region, with a diffusion coefficient having a form given by $\alpha L \dot{L}$ where $\alpha$ is an adjustable multiplier.

The LMS predictions of neutron yield are shown in Fig. 11 for two values of $\alpha$. For comparison, the yield predicted in a clean 1-D simulation is $9.9 \times 10^6$. A large increase with increasing surface roughness, followed by a decrease, is predicted for the yield as the surface roughness increases when enhanced heat loss is not included ($\alpha = 0$). The yield is predicted to increase because the shell converges farther as gas effectively leaks into the shell via mix. Further mixing reduces the central temperature and hence the neutron yield. The prediction using $\alpha = 0$ is clearly inconsistent with the measurements. When enhanced heat loss is included ($\alpha = 1$), the predicted yield varies by less than a factor of three with surface roughness because the effects of mix and heat loss nearly balance each other. Calculations with larger values of $\alpha$ (up to 5) differ little from the $\alpha = 1$ predictions. The variation with roughness shows that the yield is insensitive to the extent of the mix region which, at the time of peak neutron emission, varies between 4-μm spike growth for smooth capsules and 19-μm spike growth for capsules with initial 0.5-μm rms roughness. This lack of sensitivity arises because, as deuterated shell material moves closer to the hotter capsule center due to increasing perturbation growth, it also conducts heat away more quickly, so the temperature in the mix region stays approximately constant. The yield measurements cannot, therefore, be used to distinguish between different ways of modeling nonlinear hydrodynamic perturbation growth (DNS *vs.* LMS). The results do, however, demonstrate the importance of including enhanced heat loss in LMS modeling and also illustrate the relative importance of competing effects in determining the physical conditions in the burn region. The yield is most sensitive to the temperature in the shell which is, as these results show, insensitive to perturbation growth. However, the temperature in the shell is very sensitive to the radiation drive, as illustrated by an LMS calculation with a peak drive temperature of 231 eV (Fig. 11). For peak drive temperatures of 231–233 eV, consistent with the experimental drive, the yields predicted by LMS are very close to those predicted by DNS and also in good agreement with the data (Fig. 11).

In conclusion, we have performed the first measurements and numerical simulations of fusion yield from the gas-pusher interface of

ICF implosions. The yields predicted by DNS are found to be in quantitative agreement with the measured yields, even in the highly nonlinear regime where shell breakup occurs, without using adjustable parameters for enhanced thermal losses or mix. These measurements also show that, in a mix model based on LMS and saturation, enhanced heat loss in the mixed region is essential to match the yields. The neutron energy spectrum shows enhanced broadening, most likely arising from bulk fluid motion of the deuterated layer. The sensitivity of these measurements to the gas-pusher interface helps to test capsule implosion simulations in a way that is not possible with conventional implosions, and thereby helps to validate the models used to design ignition capsules for the NIF laser.

## References

[1] J. D. Lindl, "Development of the Indirect-Drive Approach to Inertial Confinement Fusion and the Target Physics Basis for Ignition and Gain," *Physics of Plasmas* 2, 3933 (1995).

[2] W. W. Hsing, C. W. Barnes, J. B. Beck, N. Hoffman, D. Galmiche, A. Richard, J. Edwards, P. Graham, S. Rothman, and B. Thomas, "Rayleigh-Taylor Instability Evolution in Ablatively Driven Cylindrical Implosions," *Physics of Plasmas* 4, 1832 (1997).

[3] W. W. Hsing and N. M. Hoffman, "Measurement of Feedthrough and Instability Growth in Radiation-Driven Cylindrical Implosions," *Physical Review Letters* 78, 876 (1997).

[4] P. L. Gobby, L. J. Salzer, R. D. Day, J. J. Bartos, Jr., G. Rivera, D. J. Hatch, F. P. Garcia, R. Manzanares, L. R. Foreman, and H. Bush, Jr., "Micromachining of Inertial Confinement Fusion Targets," *Nuclear Instruments and Methods for Physics Research A* 397 (1997) 183.

[5] G. I. Bell, "Taylor Instability on Cylinders and Spheres in the Small Amplitude Approximation," Los Alamos National Laboratory Technical Report LA-1321, Los Alamos Scientific Laboratory (1951).

[6] M. S. Plesset, "On the Stability of Fluid Flows with Spherical Symmetry," *Journal of Applied Physics* 25, 96 (1954).

[7] S. W. Haan, "Weakly Nonlinear Hydrodynamic Instabilities in Inertial Fusion," *Physics of Fluids B* 3, 2349 (1991).

[8] Cris W. Barnes, D. L. Tubbs, J. B . Beck, N. M. Hoffman, K. A. Klare, J. A. Oertel, R. G. Watt, T. R. Boehly, D. K. Bradley, and J. P. Knauer, "Experimental Configuration of Direct Drive Cylindrical Implosions on the OMEGA Laser," *Review of Scientific Instruments* 70, 476 (1999).

[9] D. L. Tubbs, C. W. Barnes, J. B. Beck, N. M. Hoffman, J. A. Oertel, R. G. Watt, T. Boehly, D. Bradley, and J. Knauer, "Direct Drive Cylindrical Implosion Experiments: Simulations and Data," *Lasers and Particle Beams* (to be published in 1999).

[10] Sarah A. Voss, C. W. Barnes, J. A. Oertel, R. G. Watt, T. R. Boehly, D. K. Bradley, J. P. Knauer, and G. Pien, "Gated X-Ray Framing Camera Image of a Direct-Drive Cylindrical Implosion," *IEEE Transactions on Plasma Science Triannual Issue on Images in Plasma Science* (to be published in 1999).

[11] D. P. Smitherman, R. E. Chrien, N. M . Hoffman, and G. R. Magelssen, "The Feed-out Process: Rayleigh-Taylor and Richtmyer-Meshkov Instabilities in Uniform, Radiation-Driven Foils," *Physics of Plasmas* 6, 932 (1999); D. Palmer Smitherman, R. E. Chrien, N. M. Hoffman, and G. R. Magelssen, "Feed-out Coupling of Richtmyer-Meshkov and Rayleigh-Taylor Instabilities in Stratified, Radiation-Driven Foils," *Physics of Plasmas* 6, 940 (1999).

[12] D. L. Tubbs, C. W. Barnes, J. B. Beck, N. M. Hoffman, J. A. Oertel, R. G. Watt, T. Boehly, D. Bradley, P. Jaanimagi, and J. Knauer, "Cylindrical Implosion Experiments using Laser Direct Drive," *Physics of Plasmas* 5 (to be published in 1999).

[13] C. J. Keane, G. W. Pollak, R. C. Cook, T. R. Dittrich, B. A. Hammel, O. L. Landen, S. H. Langer, W. K. Levedahl, D. H. Munro, H. A. Scott, and G. B. Zimmerman, "X-ray Spectroscopic Diagnostics of Mix in High Growth Factor Spherical Implosions," *Journal of Quantitative Spectroscopy and Radiative Transfer* 5 4, 207 (1995).

[14] O. L. Landen, C. J. Keane, B. A. Hammel, W. K. Levedahl, P. A. Amendt, J. D. Colvin, M. D. Cable, R. Cook, T. R. Dittrich, S. W. Haan, S. P. Hatchett, R. G. Hay, R. A. Lerche, R. McEachern, T. J. Murphy, M. B. Nelson, L. Suter, and R. J. Wallace, "Effects of Variable X-Ray Preheat Shielding in Indirectly Driven Implosions," *Physics of Plasmas* 3, 2094 (1996).

[15] E. M. Campbell, "Recent Results from the Nova Program at LLNL," *Lasers and Particle Beams* 9, 209 (1991).

[16] S. V. Weber, B. A. Remington, S. W. Haan, B. G. Wilson, and J. K. Nash, "Modeling of Nova Indirect Drive Rayleigh-Taylor Experiments," *Physics of Plasmas* 1, 3652 (1994); B. A. Remington, S. V. Weber, S. W. Haan, J. D. Kilkenny, S. G. Glendinning, R. J. Wallace, W. H. Goldstein, B. G. Wilson, and J. K. Nash, "Laser-Driven Hydrodynamic Instability Experiments," *Physics of Fluids B* 5, 2589 (1993).

[17] R. J. Wallace, R. L. McEachern, and W. W. Wilcox, "Laser Ablation Machining of ICF Capsules," *ICF Quarterly Report* 4, 79–86,

Lawrence Livermore National Laboratory report UCRL-LR-105821-94-3 (To obtain a copy of this document, request Document No. DE 95011970 from the National Technical Information Service, Springfield, VA 22161).

[18] R. E. Chrien, D. F. Simmons, and D. L. Holmberg, "Neutron Time-Of-Flight Ion Temperature Diagnostic for Inertial-Confinement-Fusion Experiments," *Review of Scientific Instruments* 63, 4886 (1992).

[19] M. B. Nelson and M. D. Cable, "LaNSA: A Large Neutron Scintillator Array for Neutron Spectroscopy at Nova," *Review of Scientific Instruments* 63, 4874 (1992).

[20] H. Brysk, "Fusion Neutron Energies and Spectra," *Plasma Physics* 15, 611 (1973).

[21] T. J. Murphy, R. E. Chrien, and K. A. Klare, "Neutron Time-of-Flight Signals from Expanding or Contracting Spherical Sources," *Review of Scientific Instruments* 68, 614 (1997).

[22] N. M. Hoffman, D. C. Wilson, W. S. Varnum, W. J. Krauser, and B. H. Wilde, "Multimode Hydrodynamic Stability Calculations for National Ignition Facility Capsules," 12th International Conference on Laser Interactions and Related Plasma Phenomena (Osaka, Japan, April 1995), *Laser Interations and Related Plasma Phenomena*, S. Nakai and G. H. Miley, Eds. (American Institute of Physics Press, Woodbury, New York, 1996).

[23] W. J. Krauser, N. M. Hoffman, D. C. Wilson, B. H. Wilde, W. S. Varnum, D. B. Harris, F. J. Swenson, P. A. Bradley, S. W. Haan, S. M. Pollaine, A. S. Wan, J. C. Moreno, and P. A. Amendt, "Ignition Target Design and Robustness Studies for the National Ignition Facility," *Physics of Plasmas* 3, 2084 (1996).

[24] G. Zimmerman and W. Kruer, "Numerical Simulation of Laser-Initiated Fusion," *Comments on Plasma Physics and Controlled Fusion* 11, 51 (1975).

[25] S. W. Haan, S. M. Pollaine, J. D. Lindl, L. J. Suter, R. L. Berger, L. V. Powers, W. E. Alley, P. A. Amendt, J. A. Futterman, W. K. Levedahl, M. D. Rosen, D. P. Rowley, R. A. Sacks, A. I. Shestakov, G. L. Strobel, M. Tabak, S. V. Weber, G. B. Zimmerman, W. J. Krauser, D. C. Wilson, S. V. Coggelshall, D. B. Harris, N. M. Hoffman, and B. H. Wilde, "Design and Modeling of Ignition Targets for the National Ignition Facility," *Physics of Plasmas* 2, 2480 (1995).

[26] S. W. Haan, "Onset of Nonlinear Saturation for Rayleigh-Taylor Growth in the Presence of a Full Spectrum of Modes," *Physical Review A* 39, 5812 (1989).